Biosensors and Bioelectronics 26 (2011) 2940–2947

Contents lists available at ScienceDirect

Biosensors and Bioelectronics

journal homepage: www.elsevier.com/locate/bios

Chemical and biological characterisation of a sensor surface for bioprocess monitoring

Jonathan D. Moore[a,1], Miguel A. Perez-Pardo[b,1], Jonathan F. Popplewell[c,1], Steve J. Spencer[a], Santanu Ray[a], Marcus J. Swann[c], Alex G. Shard[a], Walis Jones[d], Anna Hills[a,2], Daniel G. Bracewell[b,*]

[a] National Physical Laboratory, Hampton Road, Teddington, Middlesex, TW11 0LW, United Kingdom
[b] Department of Biochemical Engineering, University College London, Torrington Place, London, WC1E 7JE, United Kingdom
[c] Farfield Group Ltd., West Wing, Level 7, Voyager, Chicago Avenue, Manchester Airport, Manchester, M90 3DQ, United Kingdom
[d] Biopharm Enterprises Ltd., 22 Rutland Road, Harrow, Middlesex, HA1 4JW, United Kingdom

ARTICLE INFO

Article history:
Received 21 September 2010
Received in revised form
19 November 2010
Accepted 26 November 2010
Available online 4 December 2010

Keywords:
Dual polarization interferometry
Bioprocess monitoring
Biosensor
Surface characterisation
Fragment antibody

ABSTRACT

This paper describes the step-wise fabrication and characterisation of a multi-layer dual polarization interferometry (DPI) based biosensor utilising Protein G (ProG) as the bio-recognition layer for the detection of a fragment antibody (Fab′). The biosensor is capable of monitoring the concentration of Fab′ product within the extracellular medium of a fed-batch fermentation after leakage from *Escherichia coli* (*E.coli*). The activity, stability and functionality of each sensor layer were analysed *in situ* using DPI, whilst the chemical identity and homogeneity of the chemical layers were assessed *ex situ* using X-ray photoelectron spectroscopy (XPS) and secondary ion mass spectrometry (SIMS). Two different biotin linkers were found to produce hugely differing surfaces after the capture of NeutrAvidin™ (NA) and biotinylated Protein G (b-ProG). The hydrophilic $(PEG)_4$-biotin linker resulted in a surface where the b-ProG layer was deposited and organised above the NA layer producing an active and stable surface, whilst the hydrophobic LC-biotin linker generated a surface where the b-ProG layer was buried within the NA layer leading to variable surfaces and poor binding of the Fab′ target. The biosensor has a detection limit of 1.7 μg/ml with a dynamic range covering two orders of magnitude. The sensor can detect the onset of Fab′ leakage as early as 2 h following product induction, with high signal-to-noise ratios and little interference from extracellular components. Leakage of Fab′ followed a biphasic profile, switching to a more rapid rate 20 h after induction, indicating accelerated product loss and the need for cultivation harvest.

1. Introduction

The need for and use of sophisticated biosensors to monitor key product quality and performance criteria during the production of biotherapeutic drugs is being driven by multiple stakeholders in the biopharmaceutical industry. The complexity and multiple challenges inherent in bringing these products to market result in pressurised development times and processes. One initiative aimed at improving production quality and efficiency is entitled process analytical technology (PAT). This new regulatory framework advocates building real time quality testing into production processes rather than relying on the final-product testing traditionally employed (Kaiser et al., 2008).

The use of biosensors and other analytical techniques such as infra-red spectroscopy to monitor small molecule reagents and by-products such as metabolites is already established (Blankenstein et al., 1994; Landgrebe et al., 2010; Marose et al., 1999). In contrast, rapid monitoring of the production of therapeutic protein products and vaccine components is still very challenging although progress has been made, particularly for concentration analysis (Baker et al., 2002; Clementschitsch and Bayer, 2006; Mandenius et al., 2008; Marose et al., 1999). The difficulties are predominantly due to the complex nature of the cell culture environment, the problem of sensor failure due to bio-fouling of the surface and irreversible inactivation of the affinity probe due to fermentation additives.

Both off-line (where the sensor unit is not connected to the bioreactor) (Disley et al., 1999), in-line and at-line (where the sensor unit is connected to the bioreactor via tubing) (Bracewell et al., 1998; Disley et al., 1999; Gill et al., 1998; Jacquemart et al.,

* Corresponding author. Tel.: +44 (0) 20 7679 2374; fax: +44 (0) 20 7209 0703.
E-mail addresses: jonathan.moore@npl.co.uk (J.D. Moore), m.perez-pardo@ucl.ac.uk (M.A. Perez-Pardo), jpopplewell@farfield-group.com (J.F. Popplewell), steve.spencer@npl.co.uk (S.J. Spencer), santanu.ray@npl.co.uk (S. Ray), mswann@farfield-group.com (M.J. Swann), alex.shard@npl.co.uk (A.G. Shard), walisjones@yahoo.co.uk (W. Jones), anna.hills@lonza.com (A. Hills), d.bracewell@ucl.ac.uk (D.G. Bracewell).
[1] Equal credit for the preparation of this paper is due to these three authors.
[2] Current address: Lonza Biologics plc, 228 Bath Road, Slough, Berkshire, SL1 4DX, United Kingdom.

0956-5663/$ – see front matter.
doi:10.1016/j.bios.2010.11.043

2008) optical biosensor approaches to monitoring the production of protein product in bioreactors have proven popular. More recent at-line approaches have included mass spectrometric quantitation of multiple proteins within the fermentation broth (Jones et al., 2005), the use of an optical probe to measure target protein via a fluorescent fusion protein (Jones et al., 2004) and the application of flow cytometry to the analysis of cell parameters (Diaz et al., 2010).

The routine use of biosensors for monitoring therapeutic protein production in a fully, current Good Manufacturing Practice (cGMP), compliant environment is, however, still someway off. Under cGMP, manufacturing processes must be designed and controlled to ensure that the final product consistently meets pre-determined quality requirements. Process control is key to assuring this outcome and any sensor that is used to monitor a given aspect of the process must itself be validated to make certain it is fit for purpose. Therefore there is a need for well characterised surfaces to provide the basis for a robust biosensor measurement platform.

The detection system used in this study is based on an optical biosensor that uses dual polarization interferometry (DPI) to measure the opto-geometrical properties of biomolecules at the sensor surface (Cross et al., 2003). Uniquely, this biosensor technology permits analysis of thickness and density changes in addition to the mass changes occurring as layers are deposited at the sensor surface (Karim et al., 2007). In the present work we describe the development and characterisation of a sensor surface to monitor bioreactor performance during production of a fragment antibody (Fab′). Biotin tagged Protein G (b-ProG) is utilised as the biorecognition layer for the detection of Fab′ (Lian et al., 1994) and this layer is attached to the sensor surface using NeutrAvidin™ (NA), which is itself attached to the surface via an immobilised biotin linker layer. During the development of the sensor surface designed for this application, a series of surface characterisation techniques have been employed to understand the structure and functionality of each layer. High resolution chemical characterisation techniques including X-ray photoelectron spectroscopy (XPS) and secondary ion mass spectrometry (SIMS) have been employed off-line to analyse the chemical composition and distribution of the intermediate chemical layers. XPS has been used previously to provide valuable information on the conformation and behaviour of sensor surface layers (Damodaran et al., 2010a,b). The ability of DPI to enable real-time evaluation of layer structure has been exploited to allow the correlation of the structural features of each layer with its activity.

The data acquired describes the complex relationship between sensor layers showing how the choice of linker in the intermediate biotin layer affects both the binding activity of the final ProG layer, and the extent of non-specific binding (NSB) observed when bioreactor samples are measured. The advantages gained by elucidating and quantifying the key parameters that affect these performance metrics gives rise to a biosensor with a robust and reproducible surface structure and performance based on rational design, rather than derived from empirical testing. This demonstrates the importance of fully understanding the physico-chemical aspects of layer formation during biosensor development.

2. Materials and methods

2.1. Materials

All chemicals were of analytical grade. Phosphate buffered saline tablets (PBS, pH 7.4), methanol, HCl, H_2SO_4, Analar grade iso-propyl alcohol (IPA), N-[3 (trimethoxysilyl)propyl]ethylenediamine, 3-aminopropyltriethoxysilane and Tween 20 were supplied by Sigma. EZ-Link Sulfo-NHS-LC-biotin [sulfosuccinimidyl-6-(biotinamido) hexanoate] and EZ-Link NHS-$(PEG)_4$-biotin were from Pierce (Cramlington, UK). Biotinylated Protein G (b-ProtG) and NeutrAvidin™ (NA) were also purchased from Pierce (Cramlington, UK).

2.2. Dual polarization interferometry (DPI)

DPI permits the real time label-free measurement of changes in thickness and refractive index (RI) of materials up to 100 nm thick on the surface of a siliconoxynitride glass waveguide probed with a 632.8 nm laser (Cross et al., 2007, 2003). In addition, the RI measurement reflects the density of protein packing on the surface, and combined with the thickness yields a value for the mass per unit area (henceforth referred to as "mass" in ng/mm^2). All DPI measurements were performed on a dual channel AnaLight® (Farfield Group, Manchester, UK) at 20 °C.

2.3. DPI chip cleaning and silanisation

Acid cleaned chips were first immersed in methanol/HCl (aq. 37%) (50:50% v/v) for 10 min with gentle agitation including 5 s in an ultrasonic bath followed by washing in pure water (Elga HiQ). They were then soaked in conc. H_2SO_4 for 30 min, rinsed in pure water, blown dry in a nitrogen stream and dried in an oven at 110 ± 10 °C for 30 min (under vacuum for 10 min). Once cleaned, chips were allowed to cool under ambient conditions.

UV/ozone cleaned chips were washed in IPA, sonicated briefly to remove debris, then dried in a nitrogen stream and placed in a UV/Ozone Procleaner (Bioforce Nanosciences) for 20 min.

Chips were silanised with amino silanes immediately after cleaning. This was performed by soaking them (in a vacuum dried Teflon chip holder) for 1 h in a closed container of IPA, containing 4% silane by volume (made up of 33% 3-aminopropyltriethoxysilane and 66% N-[3-(trimethoxysilyl)propyl]ethylenediamine). The chips were then rinsed with IPA (without the surface drying between washes), dried in a nitrogen stream and cured in an oven at 110 ± 5 °C for 30 min.

2.4. Preparation of NeutrAvidin™ surface functionalised with biotinylated Protein G

A glass waveguide (FB 80, Farfield Group, Manchester, UK), functionalised with amine groups was mounted in the DPI instrument, and PBS flowed over the surface at 50 μl/min. Once the baseline sensor response had stabilised, ethanol/water (80% w/w) was flowed over the sensor for 30 s, followed by PBS and the baseline allowed to stabilise (this was repeated as necessary to ensure that any trace surface contamination or bubbles were removed). Elga HiQ pure water was injected for 30 s to allow the waveguide structure to be calibrated and to determine the RI of the buffer solution. To biotinylate the amine surface, 180 μl of either NHS-$(PEG)_4$-biotin or sulfo-NHS-LC-biotin (4 mg/ml, dissolved in PBS) was injected over the sensor surface at 15 μl/min and the sensor surface was then rinsed with PBS for 10 min. Loops were thoroughly washed with 50:50 (v:v) ethanol:water to remove any residual linker. Next 180 μl of NA (40 μg/ml) was injected over the biotinylated waveguide surface at a flow rate of 30 μl/min. Once the response had stabilised, 180 μl of b-ProG (50 μg/ml) was injected over the NA surface at 30 μl/min. Upon re-attaining a stable baseline, the running buffer was changed to PBS containing 0.05% (v/v) Tween 20 (PBS-T), and the baseline allowed to re-stabilise.

2.5. Fab′ detection

2.5.1. Biosensor calibration and detection

Fab′ was purified, as described elsewhere (Bowering et al., 2002), and used to calibrate the biosensor. A stock solution of Fab′ (3.96 mg/ml) was diluted in PBS-T to produce samples 1.5 μg/ml to

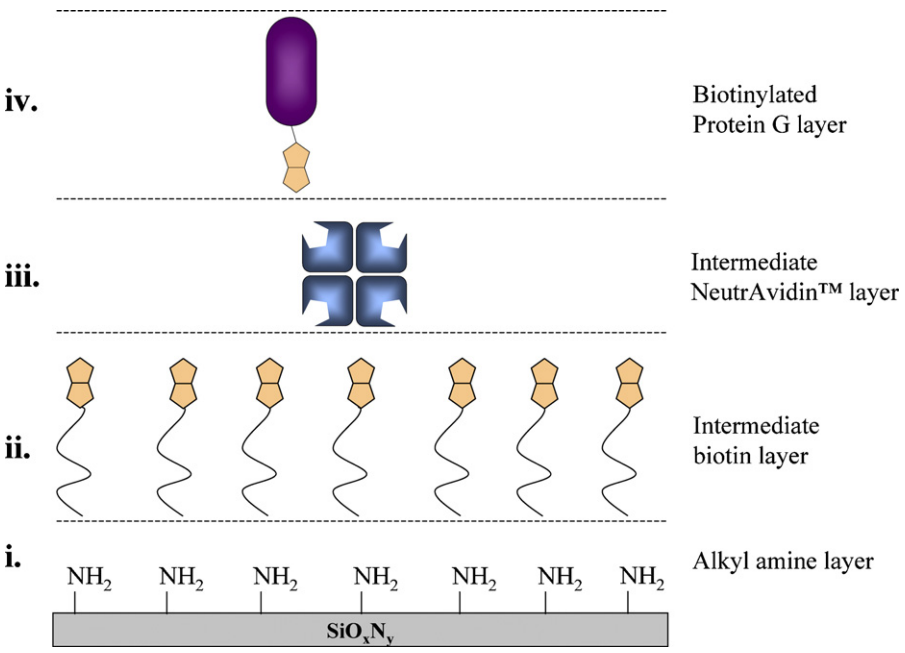

Fig. 1. Schematic of the biosensor surface layers. Schematic illustration showing the composition of the sensor surface. (i) 3-Aminopropylsiloxane (APS) layer covalently bound to the silicon oxynitride (SiO_xN_y) waveguide surface. (ii) Covalent attachment of NHS-$(PEG)_4$-biotin to APS layer via terminal amine group. (iii) Non-covalent capture of NeutrAvidin™ (NA) via biotin-avidin binding site. (iv) Non-covalent capture of Protein G (ProG) via a biotin tag.

1000 μg/ml. Aliquots (100 μl) were injected over the sensor surface at 100 μl/min which was regenerated using 50 μl injections of 20 mM di-sodium hydrogen ortho-phosphate (pH 2.5) at a flow rate of 50 μl/min.

Product leakage to the extracellular medium was measured by taking regular samples over the period of product formation following induction with isopropyl β-D-1-thiogalactopyranoside (IPTG). Fermentation broth samples (2vmL) were spun for 20 min at 13,000 rpm (Eppendorf 5415R centrifuge, Eppendorf UK, Ltd.) at 15 °C. The supernatant portion was aspirated, diluted 4-fold with PBS-T and injected over the sensor surface for 1 min at 100 μl/min, with intervening 50 μl injections of regeneration solution at a flow rate of 50 μl/min. Three separate samples were measured for each time point and results were analysed using the DPI explorer software.

2.5.2. Spike and recovery assay

The spike and recovery assay was performed using extracellular medium extracted from the fermentation broth 2 h after induction of product. Extracellular medium was used in its crude form (undiluted) or diluted either 2-fold or 4-fold using PBS-T. Purified Fab′ was added to each sample as well as the standard diluent buffer (PBS-T) to final concentrations of 0 μg/ml, 27 μg/ml, 97 μg/ml and 197 μg/ml. Samples were injected over the sensor surface as described above and the sensor response recorded. Sensor responses were converted into Fab′ concentrations using the standard curve and the percentage recovery calculated. Low levels of 'endogenous Fab′ in the extracellular medium were accounted for by subtracting the signal from the 0 μg/ml Fab′ spike samples from that of the other spiked samples.

2.6. Fermentation

2.6.1. Strain and plasmid

The industrial *Escherichia coli* (*E. coli*) strain W3110 (ATCC 27325) pre-transformed with plasmid pTTOD A33 IGS2 was generously provided by UCB Celltech (Slough, UK). The pTTOD A33 IGS2 generate A33 antibody fragments (Fab′) under specific control of the *tac* promoter. A working cell bank was prepared as described elsewhere (Bowering et al., 2002).

2.6.2. E. coli fermentation

The protocol utilised for the cultivation of pTTOD A33 has been reported previously (Tustian et al., 2007). An Applikon 201 fermenter was used instead of an LH 2000 series fermenter. The culture was sampled at various points up to 30 h after addition of the IPTG.

3. Results and discussion

3.1. Surface cleaning and silanisation

As depicted in the schematic shown in Fig. 1 the first stage of sensor preparation was the propyl amine-silanisation of the silicon oxynitride waveguide surface. In order to deposit a uniform and reproducible layer of functionalised propyl amine silane on the DPI chip surface it is necessary to expose the hydroxyl reactive groups, which are typically masked by the unwanted deposition of organic compounds (Cras et al., 1999). DPI chips were subjected to two different cleaning procedures, acid wash or a UV/ozone clean, and then analysed using contact angle measurements and XPS (descriptions of the contact angle, XPS and SIMS methods can be found in supplementary information). Initially, SIMS analysis was also used to try and identify any contaminating molecule. Measurements indicated the presence of polydimethylsiloxane (PDMS) across large parts of the chip surface after either type of cleaning procedure (data not shown). PDMS is a common surface contaminant and typically transfers from certain packaging such as gel packs. Consequently the original packaging was exchanged for polypropylene wafer containers (Fluoroware®, Entegris, Bellerica, MA) and post-cleaning, PDMS surface contamination was no longer observed. It was important to ensure surfaces were free of PDMS to first allow the chemical measurements of the surfaces to be comparable and not biased by contamination and secondly to minimise any unwanted interactions between the PDMS and protein biolayers.

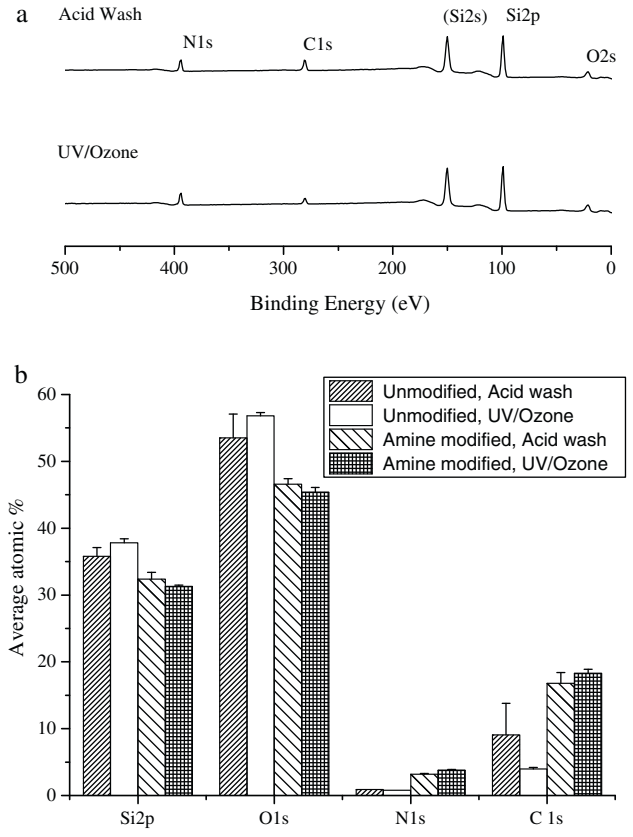

Fig. 2. XPS analysis of the sensor surface after cleaning and derivitization. (a) Representative XPS survey spectra of DPI sensor chips after either acid wash or UV/Ozone cleaning. (b) The relative amounts of key atomic species in the XPS survey spectra for unmodified and amine modified chips after either acid wash or UV/ozone cleaning. Error bars represent 1 standard deviation. Data for each element represents the average of values derived from 4 separate areas on each sensor surface.

As expected, XPS survey spectra of the surfaces indicated that the UV/ozone cleaning procedure resulted in far less contamination by carbon based material, as indicated by a smaller C1s peak (Fig. 2a and b). The contact angle measurements of the cleaned surfaces provide supporting evidence that the UV/ozone cleaning procedure is superior in removing hydrocarbon deposits. The contact angle of the unmodified DPI chip surface was $78 \pm 1.5^\circ$, decreasing to $32 \pm 4^\circ$ after the acid wash and was below the measurement limit of the instrument ($<5^\circ$) after the UV/ozone clean.

XPS analysis of the same chips after silanisation showed an increased N1s signal (above that present from the nitrogen in the SiO_xN_y waveguide), which could be attributed to the presence of amino silane. Comparison of UV/ozone and acid washed chips confirmed this increase was greater after UV/ozone cleaning as expected. This is shown in Fig. 2b.

3.2. Biotin attachment and biolayer deposition

It has been shown previously that surface attachment of streptavidin via common chemical methods such as amine coupling leads to a more heterogeneous and less structured layer than that observed for capture via a biotin linker (Su et al., 2005). The same investigators also showed that the structure of the streptavidin layer could affect the density and orientation of an additional biolayer. For this reason it was important to determine the optimal method for the immobilisation of the equivalent intermediate biolayer for the sensor surface described here. The related protein, NeutrAvidin™ (NA), which has lower nonspecific binding properties than streptavidin, was used in the development of this sensor surface. For reasons discussed above covalent attachment of NA was not considered and instead, two methods of biotin attachment were explored. The coupling reagents sulfo-NHS-LC-biotin and NHS-$(PEG)_4$-biotin were assessed for their suitability as intermediate chemical layers (stage ii in Fig. 1). Sulfo-NHS-LC-biotin contains a hydrophobic, 5-carbon chain spacer between the biotin and NHS groups, whereas NHS-$(PEG)_4$-biotin contains a hydrophilic polyethylene glycol (PEG) spacer arm.

The ability of each of the biotin layers to successfully capture and organise the intermediate NA biolayer and how well the subsequent b-ProG layer was orientated was assessed, *in situ*, using DPI measurements. Controlling and optimising the orientation of the final b-ProG layer was key to ensuring an active and robust sensor surface. As will be discussed below, differences in the NA and b-ProG layers were observed depending on which type of biotin layer was used.

Analysis of the deposition of NHS-$(PEG)_4$-biotin and sulfo-NHS-LC-biotin based on multiple chip preparations indicated that the layers formed by these two reagents were similar. The NHS-$(PEG)_4$-biotin formed a layer with mean values ($n = 18$) for thickness, mass and density of 0.64 ± 0.13 nm, 0.39 ± 0.05 ng/mm^2 and 0.62 ± 0.11 g/cm^3 respectively. The corresponding mean values ($n = 14$) for the sulfo-NHS-LC-biotin layer were a thickness of 0.49 ± 0.20 nm at a mass of 0.34 ± 0.11 ng/mm^2 and a density of 0.75 ± 0.19 g/cm^3.

Whilst the mass values for the different biotin linkers were similar, contact angle measurements revealed different hydrophobicities. Variations in hydrophobicity have been shown to affect the stability and organisation of protein layers on surfaces in applications such as micro arrays (Feng et al., 2007; Haward et al., 2010; Roach et al., 2006). The contact angles for the two biotin layers showed that using NHS-$(PEG)_4$-biotin ($74.1 \pm 2.4^\circ$) produced a significantly more hydrophilic surface than using sulfo-NHS-LC-biotin ($91.1 \pm 1.2^\circ$).

The different spacer chains appeared to make a considerable difference to the properties of the captured NA layers (stage iii in Fig. 1). Capture by the $(PEG)_4$-biotin surface resulted in an average NA layer thickness measured at 8.90 ± 1.03 nm with an average mass of 3.65 ± 0.38 ng/mm^2, whilst NA capture via LC-biotin produced an average layer thickness of 7.33 ± 1.53 nm with an average mass of 2.72 ± 0.70 ng/mm^2. Thus the flexible, hydrophilic PEG spacer allows considerably more NA to bind. Addition of NA to either biotin layer resulted in a combined layer density that was lower than the corresponding biotin layer alone. This result indicated that regardless of spacer chemistry used the NA was more than likely positioned on top of the biotin layers.

Subsequent addition of b-ProG (stage iv in Fig. 1) produced very different results as exemplified in Fig. 3a and b. Addition of b-ProG to the $(PEG)_4$-biotin/NA surface resulted in a mean ($n = 10$) thickness increase of 0.89 ± 0.40 nm and an accompanying mass increase of 0.56 ± 0.13 ng/mm^2. The density of the combined $(PEG)_4$-biotin/NA/b-ProG layers was nearly identical to that of the combined $(PEG)_4$-biotin/NA layer. When b-ProG was added to the LC-biotin/NA surface, however, the result was more variable, but showed on average a decrease in thickness of 0.26 ± 0.37 nm with a mean mass increase of 0.30 ± 0.14 ng/mm^2 (54% that of the $(PEG)_4$-biotin/NA layer) and corresponding density increase. In addition the changes in the combined layer densities observed for the two surfaces demonstrates that for the $(PEG)_4$-biotin/NA surface the b-ProG is orientated on top of the intermediate layers, whilst in the case of the LC-biotin/NA surface the b-ProG location is more variable, often burying itself within the LC-biotin/NA layers.

Fab′ binding experiments (100 μg/ml in PBS-T) were conducted using the LC-biotin and $(PEG)_4$-biotin derived ProG surfaces. The $(PEG)_4$-biotin derived ProG surface produced very consistent responses (0.681 ± 0.045 rad, % CV = 6.6), whilst the LC-biotin

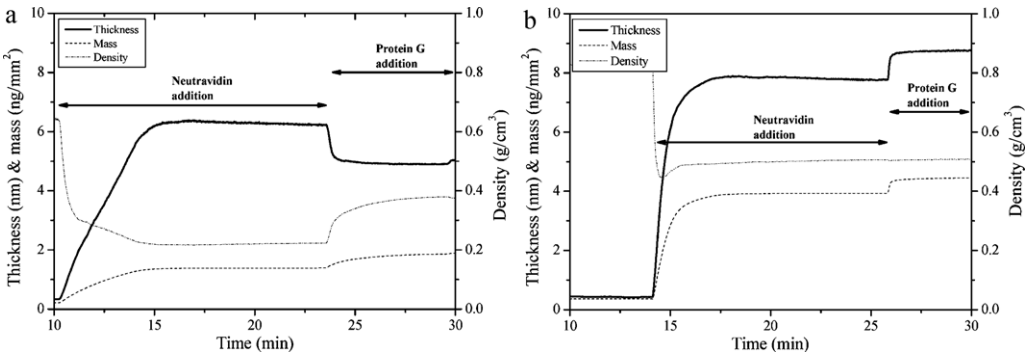

Fig. 3. Analysis of the deposition of biotin linkers and protein overlayers on the sensor surface. DPI sensorgrams showing the sequential addition of NeutrAvidin™ (NA) and b-ProG on a sensor surface modified using sulfo-NHS-LC-biotin (a) and NHS-$(PEG)_4$-biotin (b). Changes in mass, density and thickness at the surface are shown. The raw Tm phase response data (units = rad) was converted into mass data (units = ng/mm^2) using a refractive index increment of 0.183 cm^3/g.

derived surface gave highly variable sensor responses, which on average were 68% lower than those of the $(PEG)_4$-biotin derived surface (0.22 ± 0.11 rad, % CV = 55). In addition regeneration of the LC-biotin derived surface after Fab′ binding was highly variable, often stabilising at much lower values than that of the pre-measurement baseline signal indicating loss or significant rearrangement of components of the multi-layer sensor surface.

Interestingly, the mass and thickness values for the $(PEG)_4$-biotin/NA layer suggest there is a degree of castellated NA layer formation. This is borne out by the relatively low area per molecule value of 27 nm^2. In addition, consideration of the stoichiometry of the NA–b-ProG interaction, together with the thickness increase on binding b-ProG, suggests that only the upper layer of NA is available for binding. The molecular weight of NA is 60 KDa and that of ProG is 22.6 KDa, thus the mass change equates to there being 1 molecule of ProG captured per 2.35 molecules of NA, with a well spaced area per molecule for the ProG of 63 nm^2.

Having determined that NHS-$(PEG)_4$-biotin provided the best intermediate chemical layer for the addition of the subsequent biolayers, we went on to establish what degree of surface coverage was being achieved for this layer. Surface coverage is often overlooked during sensor surface development. To ensure robust sensor performance is achieved, however, reproducibly high surface coverage must be realised alongside high levels of homogeneity. Poor surface coverage and layer inhomogeneity can lead to NSB at the sensor surface and increases in the variability of the signal.

Calculating the surface coverage can be done in several different ways depending on the definition of 100% coverage. The maximum conceivable value, consisting of a layer of solid $(PEG)_4$-biotin with a thickness corresponding to its extended chain length (2.9 nm), can be determined using the RI of solid PEG (1.5, Piehler et al., 2000) and would yield a percentage surface coverage of 17%. However using an extended conformation for the calculation in this case may not be realistic as the PEG contains a hydrophobic terminal biotin which is more likely to minimise its exposure to the aqueous phase. This tallies well with the measured RI and thickness of the $(PEG)_4$-biotin layer using DPI of 1.45 and 0.64 nm respectively. Whilst thicker and less dense than obtained for the entirely hydrophobic LC-biotin it clearly indicates the molecules are prone or looped on the surface. Thus setting 100% coverage to equate to an RI of 1.5 (the maximum possible value), in the measured prone orientation the measured RI of 1.45 corresponds to a surface coverage of 72% or area per molecule of 2.0 nm^2.

To supplement the DPI data on surface coverage, a number of *in situ* prepared chips were analysed using SIMS to determine the homogeneity of the $(PEG)_4$-biotin layer SIMS mapping of a 4 mm × 4 mm area on the sensor surface was performed to look for the presence and distribution of the characteristic HS^- anion from biotin and the CNO^- anion indicative of amide bond formation. As described in the supplementary information, the SIMS mapping was performed using a Bi_3^+ primary ion beam with a 5 μm spot size. The sample was rastered over 4 mm × 4 mm using 64 × 64 individual positions. Thus, the images in Fig. 4 are constructed from 4096 individual 5 μm SIMS analyses, spaced by 62.5 μm in a square array.

The total secondary ion count image (Fig. 4a) shows that the measured sensor area is homogenous and generally free from salt contamination. The even distribution of the CNO^- anion intensity (Fig. 4b) across the area analysed indicates that the immobilisation of the $(PEG)_4$-biotin reagent is homogeneous at the measured resolution. For the HS^- anion (Fig. 4c) the mean counts/pixel is 8, for which we expect 2σ variation of ∼6. Thus the homogeneity of the HS^- anion signal is difficult to establish at this level of sensitivity. The images are consistent, however, with a homogeneous distribution and show no evidence of large-scale localisation of areas with high HS^- concentration.

3.3. Analytical performance of the sensor

The analytical performance of the sensor surface was initially assessed using purified Fab′ in PBS Tween 20 buffer (PBS-T). The change in sensor response was plotted as a function of Fab′ concentration to produce a calibration curve and was fitted using a non-linear regression analysis (standard 4 parameter dose response curve) (Fig. 5a). As is often the case for bioassays the calibration curve exhibits heteroskedasticity (a non-uniformity in the variances across the range of Fab′ concentrations tested). The analytical range of the sensor was shown to be between 10 and 1000 μg/ml of Fab′ and the limit of detection (LOD) for the purified Fab′ in buffer was 1.7 μg/ml. This detection limit corresponds to 3.4×10^{-12} molecules of Fab′ in the sample volume injected over the sensor (100 μl). The surface robustness was tested by performing multiple Fab′ injection/regeneration cycles ($n = 21$). Fab′ injections (100 μg/ml in PBS-T) over the sensor surface resulted in reproducible binding responses (average sensor response = 0.69 ± 0.03 rad), whilst ∼100% regeneration was consistently achieved after each regeneration step (average sensor response after regeneration = 0.0013 ± 0.0002 rad).

Testing of the biosensor using purified Fab′ in a simple buffer matrix provided important performance data for the sensor surface during the optimisation process. However, the final application of the new sensor required that it quantitate the same analyte within a sample matrix containing components from the cell culture medium. To assess the impact of the fermentation broth sample matrix on the performance of the biosensor, spike and recovery tests were performed. The fermentation broth was used at three levels of dilution (undiluted, 2-fold diluted and 4-fold diluted) and was spiked with three concentrations of Fab′, low (27 μg/ml), medium (97 μg/ml) and high (197 μg/ml). Table 1 compares the %

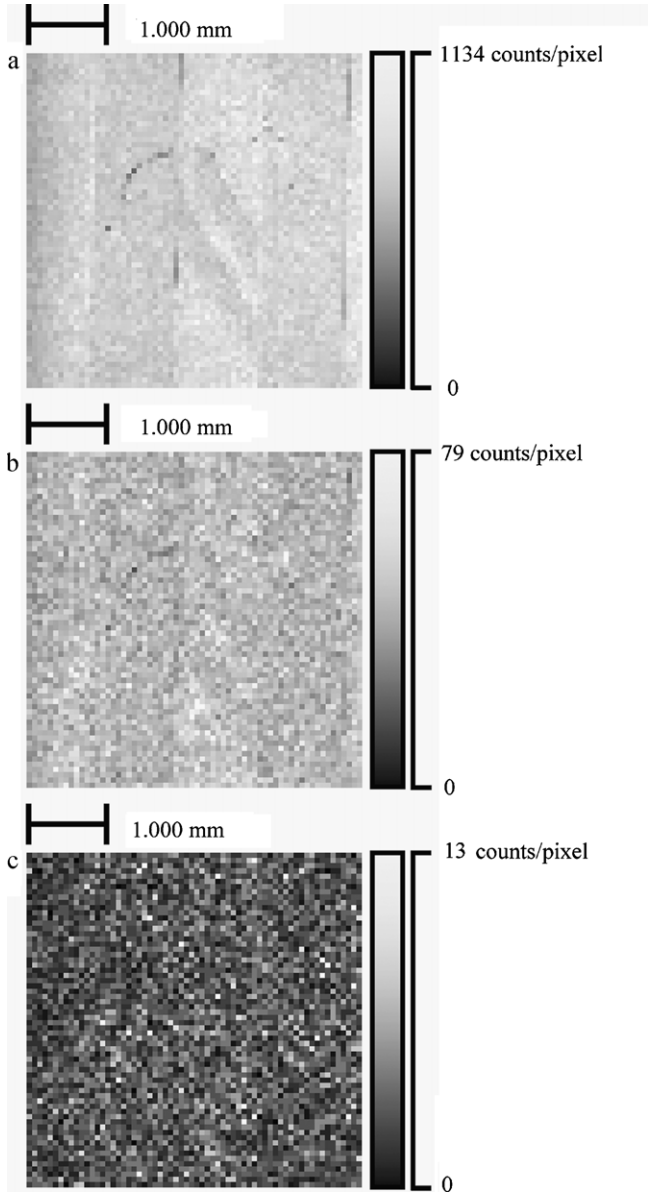

Fig. 4. SIMS images of the sensor surface after addition of the NHS-$(PEG)_4$-biotin linker. SIMS images showing the distribution of (a) total secondary ion count; (b) CNO^- (*M*: 42.02); (c) HS^- (*M*: 33.07). The two darker bands running vertically in image (a) are due to the sensing regions of the DPI waveguide. The cladding and sensing regions have different secondary ion yields.

recoveries obtained for these samples. The results indicate that the biosensor performs satisfactorily when broth samples are diluted 4-fold using the standard diluent (PBS-T), however the % recoveries for both the undiluted and 2-fold diluted broth samples indicate that for these samples, components within the sample matrix are compromising the biosensor response. Interestingly, for all types of broth sample used (undiluted, 2-fold diluted and 4-fold diluted), complete regeneration of the sensor surface was achieved indicating that the differences in the % recoveries are most likely due to sample matrix components interfering with the analyte itself, rather than irreversibly inactivating the sensor surface.

3.4. Detection of Fab′ leakage from cells in an *E. coli* fermentation run

The fully characterised sensor surface was used to successfully carry out monitoring of a 20 l, *E. coli*, fed-batch fermentation run producing the Fab′ of interest. The sensor was used to measure the onset of leakage of Fab′ product from the *E. coli* cells after induction. For the purpose of the test the fermentation run was allowed to proceed beyond the time point when Fab′ leakage had been detected, and samples were harvested for testing up to 30 h after induction. Normally detection of the onset of Fab′ leakage would prompt the immediate cessation of the fermentation run and the cells would be harvested thereby minimising product loss and degradation.

As described above, all fermentation broth samples had to be diluted 4-fold using the running buffer PBS-T before analysis. Assessment of neat broth and other dilutions had shown this was the minimum dilution necessary to ensure that the extracellular components did not significantly affect the sensor's performance. This dilution factor is similar to that used for other at-line monitoring sensors (Jacquemart et al., 2008).

Despite the high levels of non-target proteins and other biological material present in the broth samples, increasing Fab′ concentration in the extracellular medium was detected with high signal-to-noise and regeneration of the sensor surface was found to be sufficient for broth samples up to 30 h post-induction (Fig. 5b). Measurement of broth samples beyond this time were hampered as the sensor surface could no longer be fully regenerated indicating partial fouling of the surface. In parallel studies of the later stages of fed-batch fermentations using this *E. coli* strain, increases in the viscosity of the extracellular medium and the appearance of a higher quantity of particulate matter (diameters of ~0.1 μm) have been observed, indicating accelerated cell breakage and release of intracellular components such as DNA (unpublished results). The presence of cellular debris, not removed by centrifugation and released DNA may well be the cause of the increased sensor surface fouling observed after 30 h post-induction.

Critically, however, the onset of Fab′ leakage was detected much earlier than this, from 2 h onwards, when sensor performance

Table 1
Biosensor spike and recovery of Fab′ in fermentation broth.

Sample	Spike level (μg/ml)	[a]Expected conc. (μg/ml)	Observed conc. (μg/ml)	Recovery (%)
4-Fold diluted fermentation broth	Low (27)	29.6 ± 1.2	24.4 ± 2.7	82.4 ± 9.5
	Med (97)	85.9 ± 0.5	71.3 ± 3.7	83.0 ± 4.0
	High (197)	154.6 ± 2.2	137.9 ± 5.9	89.1 ± 3.7
2-Fold diluted fermentation broth	Low (27)	29.6 ± 1.2	15.9 ± 2.9	53.7 ± 10.0
	Med (97)	85.9 ± 0.5	56.1 ± 2.2	65.3 ± 2.6
	High (197)	154.6 ± 2.2	92.7 ± 1.9	60.0 ± 1.5
Undiluted fermentation broth	Low (27)	29.6 ± 1.2	12.9 ± 2.8	43.5 ± 9.5
	Med (97)	85.9 ± 0.5	40.5 ± 3.4	47.1 ± 4.0
	High (197)	154.6 ± 2.2	80.2 ± 5.1	51.9 ± 3.4

Expected and observed Fab′ concentrations measured using the biosensor after spiking into undiluted, 2-fold diluted and 4-fold diluted fermentation broth. The % recovery values for each spike level are also shown. Each value represents the average of 3 measurements and the errors are 1 standard deviation.

[a] The expected concentrations are determined by conversion of the raw biosensor response using the standard curve for analyte spiked into the standard diluent buffer (PBS-T).

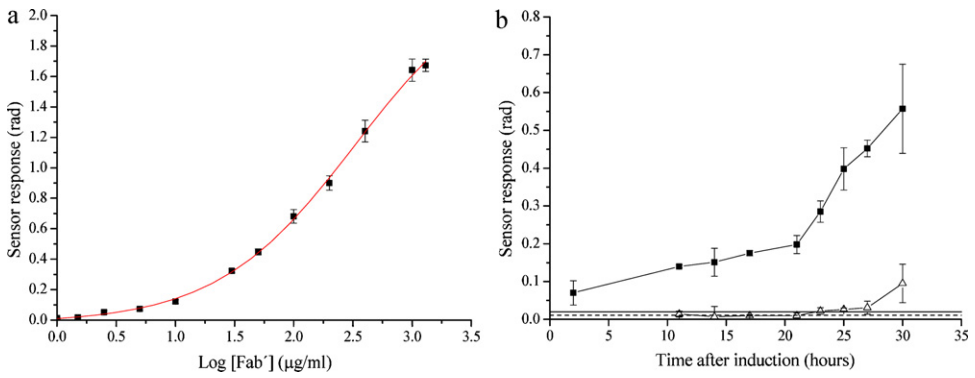

Fig. 5. Biosensor performance in standard buffer and analysis of a fermentation run. (a) Steady state binding response of biosensor for purified Fab′ (1.5–1300 μg/ml) in PBS-T buffer. All data points represent triplicate measurements and error bars represent 1 standard deviation. Curve fitting was performed using a four-parameter sigmoidal dose-response equation using non-linear regression analysis (Origin v7, OriginLab). (b) Response observed on the active channel after injection of diluted broth samples taken between 2 and 30 h after induction of Fab′ expression (filled squares) and subsequent surface regeneration (open triangles). Each data point represents the average of 3 measurements and the error bars are 1 standard deviation (where errors bars are not visible they are hidden by the data point). The horizontal dotted line represents the background signal for broth samples (30 min post induction Fab′ expression levels). The solid, horizontal line corresponds to the cut off signal level for Fab′ leakage above which the biosensor can robustly detect Fab′ in the extracellular medium. (This threshold value represents the 95 percentile above background.)

and surface regeneration have been shown to still be appropriate (Fig. 5b). The threshold signal indicating Fab′ leakage was validated at 0.020 rad for the sensor surface. This value represents the 95th percentile above background provided by analysis of the 30 min post-induction broth samples ($n = 9$). It was not possible to use pre-induction broth samples to estimate the background signal due to the fact that certain components within the extracellular medium caused inactivation of the sensor surface. Upon induction these components are rapidly metabolised by the cells as they over express the protein such that shortly after induction (~30 min) their concentration within the broth drops to levels permitting measurement.

In addition, to understand the effects of the sample matrix on the biosensor's performance it was important to ensure that the matrix used for the background measurements was representative of that in which the Fab′ was present. Because large changes in the matrix are observed in the short time period before and after induction it is inappropriate to use pre-induction samples as the basis for estimating the background signal (Huisman and Zambrano, 1996; Kolter et al., 1993).

Individual measurements, including sample injection, signal collection and sensor surface regeneration could be performed in a 2 min time period. This compares favourably to a typical reference HPLC method, which takes ~7 min to analyse a single sample and is roughly equivalent to the response time for an optical biosensor developed previously, which used initial rate determinations to monitor analyte concentrations (Holwill et al., 1996). Although this biosensor, like all surface-based affinity sensors, cannot be used for continuous monitoring due to the need for surface regeneration, the measurement turnaround time is sufficiently fast to enable near-continuous analysis of the fermentation process.

It is clear that the rate of product loss due to leakage from the cells' periplasmic space increases after 20 h post-induction. This observation is in agreement with the findings of a previous report on the leakage rates of Fab′ from *E. coli* in high and low carbon source feed rate, fed-batch fermentation systems (Backlund et al., 2008). In the first 20 h after induction the Fab′ concentration detected in the extracellular medium rose to 60 mg/l, and increased more rapidly in the following 10 h to 294 mg/l. At this 30 h time point the level of Fab′ in the medium represents roughly 35% of the typical total protein concentration (835 mg/l) for this expression system (personal communication); a significant amount of product loss. Understanding the degree and rate of product loss is of critical importance to selecting the best harvest point for these bioprocesses.

4. Conclusions

A DPI based sensor surface has been developed that enables direct monitoring of the leakage of Fab′ from *E. coli* during fed-batch fermentation. In this study, we have shown how DPI can be used alongside surface chemical analytical techniques to scrutinise and understand the properties and activity of each layer on the sensor surface.

The structural properties and activity of the sensor's biolayers were shown to be critically dependent on the type of biotin linker used. Analysis of the thickness and density changes observed during the deposition of the NA and b-ProG layers on the two biotin linker layers allowed the differences in sensor activity to be understood and explained in terms of the geometry of these layers.

The biosensor has been shown to be sensitive down to 1.7 μg/ml of Fab′ with low interference due to non-specific binding (NSB) and good percentage recovery in 4-fold diluted broth. Routine analysis of fermentation broth samples has been demonstrated and leakage of Fab′ material into the extracellular medium was successfully monitored over the duration of the fermentation process. In addition data from the biosensor has identified a distinct change in the rate of Fab′ leakage 20 h post-induction, pre-empting higher rates of product loss over the remainder of the fermentation run.

This study has shown the importance of the underlayer properties on biosensor performance and has shown how the use of chemical and biological analysis of each sensor layer facilitates rapid development of an optimised biosensor for use in complex matrices. The work described here focussed on bioprocess monitoring, however, the principles we have explored are relevant to many biosensors employing multi-layer sensing surfaces for detecting analytes within other complex matrices such as serum.

Acknowledgements

This work was supported in part by the Department of Business Innovation and Skills (BIS) through the National Measurement Office's Measurement for Innovators (MfI) Programme and by BioPharm Enterprises Ltd. and Farfield Group Ltd., as part of a Joint Industry Project (JIP) with NPL. The support of the Engineering and Physical Sciences Research Council (EPSRC) Innovative Manufacturing Research Centre (IMRC) initiative for the "IMRC in Bioprocessing" is acknowledged gratefully as is the support of Biopharm Enterprises Ltd. for an Engineering Doctorate (EngD) for Miguel Perez-Pardo. We wish to thank Alan Hughes for assistance

with the contact angle measurements and Shaukat Ali and Balasundaram Bangaru for assistance conducting fermentation runs.

Appendix A. Supplementary data

Supplementary data associated with this article can be found, in the online version, at doi:10.1016/j.bios.2010.11.043.

References

Backlund, E., Reeks, D., Markland, K., Weir, N., Bowering, L., Larsson, G., 2008. J. Biotechnol. 135 (4), 358–365.
Baker, K.N., Rendall, M.H., Patel, A., Boyd, P., Hoare, M., Freedman, R.B., James, D.C., 2002. Trends Biotechnol. 20 (4), 149–156.
Blankenstein, G., Spohn, U., Preuschoff, F., Thommes, J., Kula, M.R., 1994. Biotechnol. Appl. Biochem. 20, 291–307.
Bowering, L.C., Bracewell, D.G., Kesharvarz-Moore, E., Hoare, M., Weir, A.N., 2002. Biotechnol. Prog. 18 (6), 1431–1438.
Bracewell, D.G., Gill, A., Hoare, M., Lowe, P.A., Maule, C.H., 1998. Biosens. Bioelectron. 13 (7–8), 847–853.
Clementschitsch, F., Bayer, K., 2006. Microb. Cell Factories, 5.
Cras, J.J., Rowe-Taitt, C.A., Nivens, D.A., Ligler, F.S., 1999. Biosens. Bioelectron. 14 (8–9), 683–688.
Cross, G.H., Freeman, N.J., Swann, M.J., 2007. In: Marks, R.S., Lowe, C.R., Cullen, D.C., Weetall, H.H., Karube, I. (Eds.), Handbook of Biosensors and Biochips. Wiley, New York, pp. 549–568.
Cross, G.H., Reeves, A.A., Brand, S., Popplewell, J.F., Peel, L.L., Swann, M.J., Freeman, N.J., 2003. Biosens. Bioelectron. 19 (4), 383–390.
Damodaran, V.B., Fee, C.J., Popat, K.C., 2010a. Appl. Surf. Sci. 256 (16), 4894–4901.
Damodaran, V.B., Fee, C.J., Ruckh, T., Popat, K.C., 2010b. Langmuir 26 (10), 7299–7306.
Diaz, M., Herrero, M., Garcia, L.A., Quiros, C., 2010. Biochem. Eng. J. 48 (3), 385–407.
Disley, D.M., Morrill, P.R., Sproule, K., Lowe, C.R., 1999. Biosens. Bioelectron. 14 (5), 481–493.
Feng, J., Wong, K.Y., Lynch, G.C., Gao, X.L., Pettitt, B.M., 2007. J. Phys. Chem. B 111 (49), 13797–13806.
Gill, A., Bracewell, D.G., Maule, C.H., Lowe, P.A., Hoare, M., 1998. J. Biotechnol. 65 (1), 69–80.
Haward, S.J., Shewry, P.R., Miles, M.J., McMaster, T.J., 2010. Biopolymers 93 (1), 74–84.
Holwill, I., Gill, A., Harrison, J., Hoare, M., Lowe, P.A., 1996. Process Contr. Qual. 8 (4), 133–145.
Huisman, G., Zambrano, S.D.M.R.K., 1996. In: Neidhardt, F.C.I.R., Ingraham, J., Lin, E., Low, K., Magasanik, B., Reznikoff, W., Riley, M., Schaechter, M., Umbarger, H. (Eds.), *Escherichia coli* and *Salmonella*: Cellular and Molecular Biology. ASM Press, Washington, DC, pp. 1672–1682.
Jacquemart, R., Chavane, N., Durochcr, Y., Hoemann, C., De Crescenzo, C., Jolicoeur, M., 2008. Biotechnol. Bioeng. 100 (1), 184–188.
Jones, J.J., Bridges, A.M., Fosberry, A.P., Gardner, S., Lowers, R.R., Newby, R.R., James, P.J., Hall, R.M., Jenkins, O., 2004. J. Biotechnol. 109 (1–2), 201–211.
Jones, J.J., Wilkins, C.L., Cai, Y., Beitle, R.R., Liyanage, R., Lay Jr., J.O., 2005. Biotechnol. Prog. 21 (6), 1754–1758.
Kaiser, C., Pototzki, T., Ellert, A., Luttmann, R., 2008. Eng. Life Sci. 8 (2), 132–138.
Karim, K., Taylor, J.D., Cullen, D.C., Swann, M.J., Freeman, N.J., 2007. Anal. Chem. 79 (8), 3023–3031.
Kolter, R., Siegele, D.A., Tormo, A., 1993. Annu. Rev. Microbiol. 47, 855–874.
Landgrebe, D., Haake, C., Hopfner, T., Beutel, S., Hitzmann, B., Scheper, T., Rhiel, M., Reardon, K.F., 2010. Appl. Microbiol. Biotechnol. 88 (1), 11–22.
Lian, L.Y., Barsukov, I.L., Derrick, J.P., Roberts, G.C., 1994. Nat. Struct. Biol. 1 (6), 355–357.
Mandenius, C.F., Wang, R., Alden, A., Bergstrom, G., Thebault, S., Lutsch, C., Ohlson, S., 2008. Anal. Chim. Acta 623 (1), 66–75.
Marose, S., Lindemann, C., Ulber, R., Scheper, T., 1999. Trends Biotechnol. 17 (1), 30–34.
Piehler, J., Brecht, A., Valiokas, R., Liedberg, B., Gauglitz, G., 2000. Biosens. Bioelectron. 15 (9–10), 473–481.
Roach, P., Farrar, D., Perry, C.C., 2006. J. Am. Chem. Soc. 128 (12), 3939–3945.
Su, X.D., Wu, Y.J., Robelek, R., Knoll, W., 2005. Langmuir 21 (1), 348–353.
Tustian, A.D., Salte, H., Willoughby, N.A., Hassan, I., Rose, M.H., Baganz, F., Hoare, M., Titchener-Hooker, N.J., 2007. Biotechnol. Prog. 23 (6), 1404–1410.